# Miniature field deployable Terahertz source

Mark G. Mayes*

Applied Physical Electronics L.C.
P.O. Box 341149 Austin TX 78734

## ABSTRACT

Developments in terahertz sources include compacted electron beam systems, optical mixing techniques, and multiplication of microwave frequencies. Although significant advances in THz science have been achieved, efforts continue to obtain source technologies that are more mobile and suitable for field deployment. Strategies in source development have approached generation from either end of the THz spectrum, from up-conversion of high-frequency microwave to down-conversion of optical frequencies. In this paper, we present the design of a THz source which employs an up-conversion method in an assembly that integrates power supply, electronics, and radiative component into a man-portable unit for situations in which a lab system is not feasible. This unit will ultimately evolve into a ruggedized package suitable for use in extreme conditions, e.g. temporary security check points or emergency response teams, in conditions where THz diagnostics are needed with minimal planning or logistical support. In order to meet design goals of reduced size and complexity, the inner workings of the unit ideally would be condensed into a monolithic active element, with ancillary systems, e.g. user interface and power, coupled to the element. To attain these goals, the fundamental component of our design is a THz source and lens array that may be fabricated with either printed circuit board or wafer substrate. To reduce the volume occupied by the source array, the design employs a metamaterial composed of a periodic lattice of resonant elements. Each resonant element is an *LC* oscillator, or tank circuit, with inductance, capacitance, and center frequency determined by dimensioning and material parameters. The source array and supporting electronics are designed so that the radiative elements are driven in-phase to yield THz radiation with a high degree of partial coherence. Simulation indicates that the spectral width of operation may be controlled by detuning of critical dimensions. We discuss simulation results and frequency response for a single element and the source array, and the component density necessary to achieve target output intensities. After obtaining the primary objective of a designing a compact fieldable THz source, the secondary goal is developing a fabrication recipe which draws upon existing methods in PCB/integrated circuit manufacturing to obtain a device that may be produced at volume with high yield.

**Keywords:** Terahertz, metamaterial, split ring resonator, helical antenna, photolithography, sol-gel

## 1. INTRODUCTION

*A. Background*

Radiation in the THz regime, 0.3 to 30 THz, presents a unique challenge as it does not easily give way to approaches that are all-electronic or all-optical. Applications include non-penetrating radiography for high-contrast images without the ionizing effects caused by x-ray, to provide a complementary technology for soft tissue imaging and security screening. Spectroscopy is another valuable application due to the strong interaction of THz with organic compounds for chemical signatures in detection and identification. THz spectroscopy is widely documented as a countermeasure against concealed explosives and contraband, and for detection and neutralization of biohazards such as anthrax. Because this frequency range offers significant benefits for numerous applications, much effort has been invested in development of smaller cheaper THz technologies. Early sources e.g. synchrotron are electron beam machines which generate radiation through acceleration and deceleration of electrons. The free electron laser employs a similar mechanism to generate radiation hence relies upon e-beam technologies. Due to the size requirements for obtaining specific kinetic energies, and the footprint occupied by ancillary systems, limited size reductions are possible for e-beam sources. One notable development, however, uses modified electron optics based on a scanning electron microscope design in order to produce a THz laser for medical applications [3].

* Send correspondence to mgmayes@apelc.com

*B. Metamaterials*

The radiative component in our design is based upon an array of subwavelength structures termed *metamaterial* or *negative index material*. NIM originated with the consideration of a hypothetical material defined by a negative permittivity and negative permeability at a given frequency. Theoretical treatments of the material's interaction with an electromagnetic field gave rise to counterintuitive and controversial results [4]. Recent experiments in electromagnetic materials corroborated early theoretical predictions, notably, sub-wavelength imaging [5, 6]. These engineered materials are variously named NIM, *left-handed materials*, or metamaterials. The negative permittivity and permeability of NIM yield a negative index of refraction at a specific frequency so that light incident upon a NIM interface is refracted towards the normal axis rather than away. Left-handed materials are so labeled because power propagation is in the opposite direction indicated by the right-hand rule.

One way to create a metamaterial is through a uniformly mixture of nanoparticles in a liquid substrate, e.g. epoxy or a thermoset compound. Nanoparticles are typically metallic spheres or air voids, with diameters several magnitudes smaller than a particular wavelength of interest, i.e. $\lambda_0$. The inclusions are distributed throughout the host substrate so that the composite matrix has a lattice spacing considerably less than $\lambda_0$. Thus, radiation at $\lambda_0$ interacts macroscopically with the metamaterial, without regard for its microscopic structure. In this manner, a composite material may be engineered to manifest optical effects for a particular range of frequencies. The term metamaterial encompasses materials with subwavelength structures whose aggregate interacts in a macroscopic manner with radiation of a specific wavelength(s). The split ring resonator (SRR) geometry discussed in this paper falls under this heading and is developed in greater detail in the following section. Metamaterials that serve as THz active elements, i.e. source or detector, are well established and promise to yield new technologies that are smaller, cheaper, and more efficient than previous methods [7].

## 2. DESIGN

The design presented in this paper employs a hybrid approach that draws upon technologies from both microwave and photonics, with a metamaterial comprised of THz resonators combined with a lens array, to obtain a highly-directive THz active element in a monolithic element. This design was developed to enable fabrication via standard optical lithography and silicon manufacturing protocols. Although the design is based upon a nominal frequency of 1 THz, the concept may be applied with dimensional modifications to a wide range of operating frequencies, due to the extensibility of electricity and magnetism. The metrics used to quantify performance are the gain and half power beam width.

The design and assembly for the APELC device consists of three components—driver circuitry, source array, and directive optics. The driver circuit conditions the input from the power source through conversion of low-frequency signal to high-frequency microwave using commercial off-the-shelf (COTS) components initially then transitioning to custom geometries. The THz source is a grid of SRR elements driven in a manner that optimizes constructive addition of the resulting radiation. The directive element in this design is a helical antenna array constructed with THz scale elements, i.e. 1 mm to 10 micron for 0.3 to 30 THz.

### 2.1. Driver circuitry

The driver electronics are the circuits that source the array of THz resonators. The circuit is also designed to enable the system to function as both a transmitter and receiver by supporting dual mode operation of the SRR and antenna elements. The basic element is the parametric amplifier design from microwave devices—the familiar *LC* tank circuit with resonant frequency $f_0 = 1/2\pi\sqrt{LC}$ in figure 1.

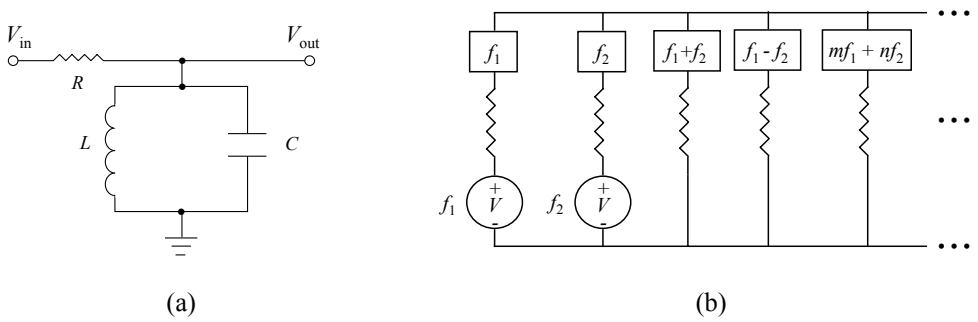


**Figure 1**. Parametric amplifiers (a) Tank circuit (b) Manley-Rowe circuit

Because the tank circuit is a resonant device, it operates at center frequency $f_0$ and rejects other frequencies. The driver circuit is formed by a cascade of *LC* tank circuits. The front end operates at microwave frequencies and sources the higher frequency cascades to obtain the THz input required to excite the active element. Connecting tanks in parallel is a means to achieve frequency conversion [8, 9]. The Manley-Row cascade (MRC) in figure 1(b) consists of a number of tank circuits in parallel to obtain multiples of the input frequency. In this manner a low frequency is up-converted to a high frequency. The front end of the MRC is constructed with standard microwave components. Once conversion extends beyond the limits of COTS components, the signal is coupled to an MRC of SRR elements which are fabricated in decreasing geometries to achieve higher frequency operation. The SRR's are initially fabricated on a printed circuit board then patterned on a silicon substrate once PCB dimensional limits are reached.

## 2.2. Split Ring Resonator

The split ring resonator in figure 2 is formed by concentric geometries fabricated by patterning and etching metal on dielectric to produce another manifestation of the tank circuit. This geometry has been successfully exploited by numerous THz workers and is notable for its high *Q* (e.g. thousands), wide fee spectral range (e.g. 6 THz), and straightforward fabrication. The behavior of the SRR as a THz metamaterial has been characterized by numerous researchers [10,11,12,13,14]. Frequencies in the neighborhood of 100 THz are reported from structures on the order of micron to submicron that are fabricated through electron beam lithography. Frequencies in the range of 10's of THz are generated by larger geometries and may be fabricated by standard optical lithography. Use of the SRR in the THz has progressed to the point where design guidelines have been defined, notably in [14]. Marqués *et al* formulate the geometry in terms of the dimensions and material parameters necessary to achieve the inductance and capacitance to obtain a specific resonant frequency.

The circuitry of the SRR array in this paper is designed to synchronously distribute the input signal to each element, so that array elements oscillate in-phase in order to achieve a high degree of partial coherence across the array. Signal timing is achieved by sourcing and grounding each element with traces of near-identical impedance and length to attain uniform delay throughout the array. To verify operation, Remcom XFDTD is used to simulate the device and effects of variation in critical dimensions. The SRR and results are shown in figure 2.

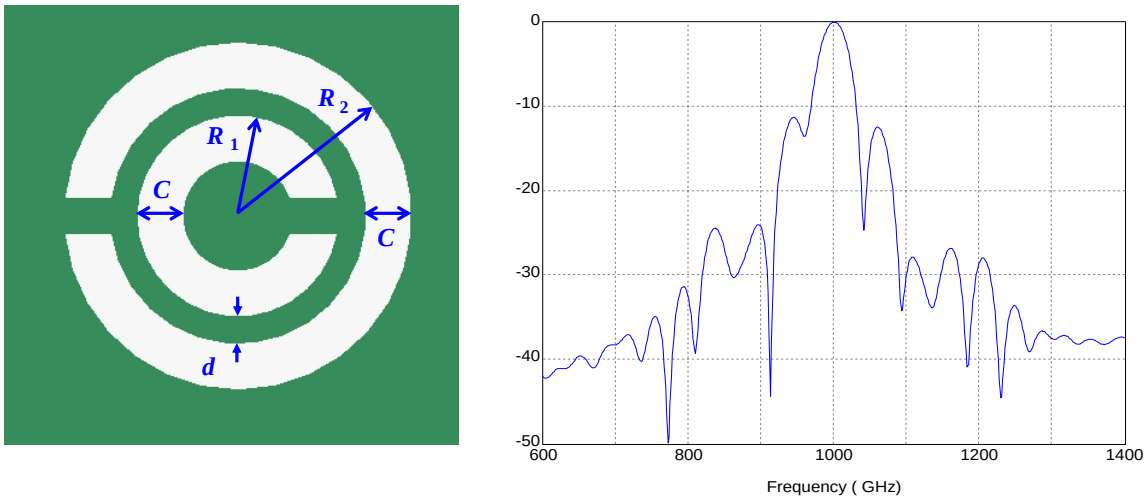


(a) (b)

**Figure 2**. (a) Split ring resonator geometry and dimensional parameters after Marqués [14], (b) frequency response of SRR with center at 1 THz.

To achieve 1 THz operation , the SRR was dimensioned with parameters summarized in Table 1.

**Table 1**. Simulation parameters for geometry in figure 2a, with inner radius (*IR*), outer radius (*OR*), and metal thickness ( *z* ).

| | **IR** | **OR** | **z** |
|---|---|---|---|
| | micron | micron | micron |
| **Inner ring** | 60 | 90 | 20 |
| **Outer ring** | 110 | 140 | 20 |
| ***C*** | 30 | micron | |
| ***d*** | 20 | micron | |

In this design, the structure is fabricated on a two-metal substrate, with metal 1 supplying input and ground connections, and metal 2 providing ring material, as depicted in figure 3. Choice of fabrication substrates include printed circuit board and semiconductor substrate. While a PCB substrate offers a robust option, smaller geometries and critical dimensions may be reproduced with tighter tolerances on a wafer substrate. The objective is to print the array with precision in ring dimensions to achieve the desired resonant frequency and *Q*, and precision in metal 1 traces so that array resonates in unison. Ultimately, the choice of substrate is determined by customer specifications; lower frequencies with wavelengths in the millimeters may be obtained on PCB.

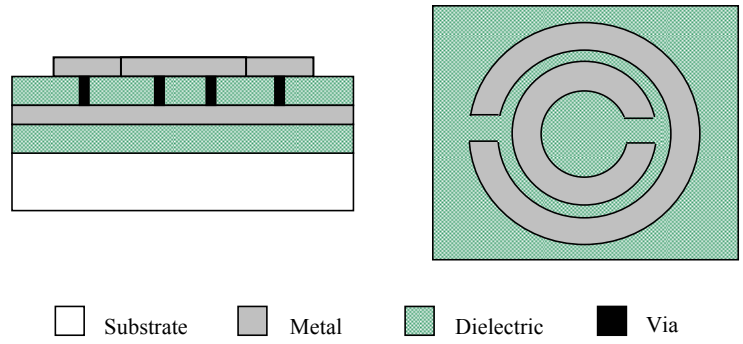


**Figure 3**. SRR from figure 2 fabricated in a two metal process. First metal provides input and ground traces. The SRR is fabricated by patterning second metal.

## 2.3. THz Helical antenna array

The helix is an antenna that yields higher gain with more windings. The resonance of the helical antenna occurs at the wavelength that matches the circumference of the circular cross-section. The operational frequencies of the antenna are determined by several parameters, including the precision of the windings with respect to the desired wavelength, the spacing between turns, and the total number of turns. Optimal design parameters for this antenna are given in comprehensive detail by its inventor, J.D. Kraus, in [15]. A significant benefit of the helical antenna is that the conductor is wound in a circular manner rather than printed as a linear structure, so that its cross-sectional footprint is reduced by a factor of $1/\pi$ ( $\approx 32\%$) in comparison to a trace of length $\lambda$. This allows higher integration density in the present implementation. Second, because the antenna is a resonant device, its center frequency may be closely matched to that of the SRR array. Moreover, the *Q* of this antenna can be controlled through a detuning of the winding circumference to support a wider bandwidth if necessary. Finally, the helical geometry is extensible across the range of electromagnetic frequencies and has been applied with success to THz radiation [16]. To create the monolithic active element, the array of helical elements is fabricated over the source array. The coupling of the SRR fabric to free space is bi-directional, as the antenna array may function as both a transmitter and receiver. To characterize the scale of the geometry, antenna dimensions are tabulated for several frequencies in the THz regime.

**Table 2**. THz frequencies and wavelengths and helix outer diameter (*OD*)

| **Frequency** THz | **Wavelength** micron | **Helix OD** micron |
|---|---|---|
| 0.50 | 600.00 | 190.99 |
| 1.00 | 300.00 | 95.49 |
| 2.50 | 120.00 | 38.20 |
| 5.00 | 60.00 | 19.10 |

As seen in the table, feature dimensions for 5 to 0.5 THz vary from 60 to 600 microns. In the current state of fabrication and photolithography, these dimensions are quite large and are easily within reach of legacy exposure tools.

In keeping with the goal of maintaining standardized processing, the three-dimensional helix is fabricated with a stack of two-dimensional structures, through a sequence of deposition, patterning, and etch steps. The first structure fabricated is a partial turn (i.e. winding). In the present implementation, the winding geometry is hexagonal when viewed end-on. The next step adds a metal contact to provide connectivity between layers. The contact is fabricated at angle as shown in figure 4, to complete a single turn in the winding geometry.


**Figure 4**: A single helix winding. The hexagon perimeter equals wavelength. For center frequency of 1 THz, λ = 300 micron. Spacing *h* between turns is 0.225λ (67.50 micron) for optimal design.

As successive layers are stacked, the aggregate structure approximates a helical geometry. This geometry is modeled in Remcom XFDTD to establish that the electrical behavior is that of a circular helix. Figure 5 depicts the THz antenna in the XFDTD environment.

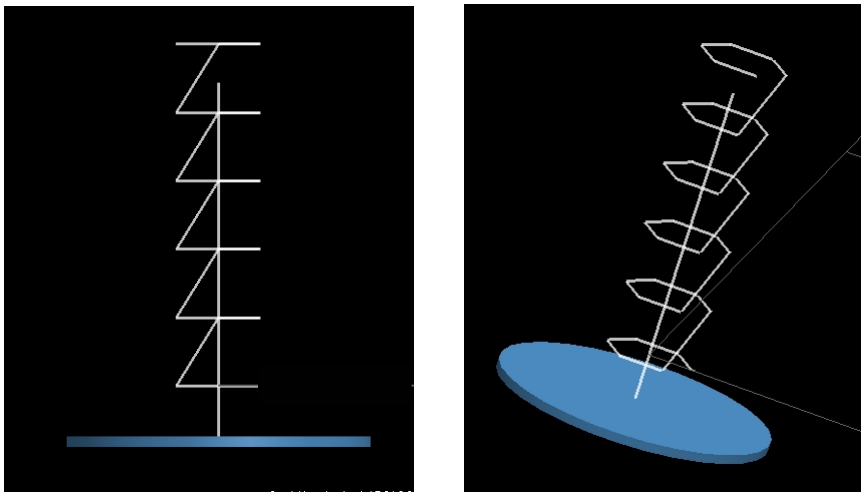

**Figure 5**: Antenna designed for 1 THz. Helix diameter is 95.49 micron, and total height (six turns) is 405 micron. Ground plane in blue, with center-conductor rod extending ground.

As illustrated in the figure, a center ground rod is added to extend the ground plane through the structure, for enhanced guiding and focusing of the field. Gain and spatial field plots for this geometry are presented with simulation results in following sections.

## 2.4. Fabrication method

The THz antenna in figure 5 is fabricated in twelve layers, alternating the hexagonal trace layer with contact. For 1 THz, the contact lead is set to a length of 67.50 micron to achieve the 0.225λ spacing in Kraus' design rule. Fabrication of this structure may be implemented in several ways. One method follows a traditional manufacturing sequence—metal deposition, patterning, etch, and film deposition. An alternative process is based on a sol-gel technique. In this method, a hybrid organic-inorganic glass sol-gel is exposed with UV to combine organic polymers with silica by way of polymer lithography [17]. The sol-gel is prepared with photoactive organic polymers containing metallic inclusions for the formation of conductive traces. A second sol-gel of organic-inorganic glass compound forms the substrate. The planar structure in figure 4 is inscribed into the material by exposure through a photomask. Exposure and post-exposure bake produce polymerization in the exposed material to reproduce the photomask geometries.

Use of the sol-gel process not only provides an alternative to traditional methods, but allows faster prototyping cycles and production runs. Because the sol-gel provides both the photoactive component and substrate, film deposition and patterning are consolidated into a single processing node. The post-bake develop solution removes unexposed substrate to supplant the etch function. A sol-gel is a spin-on coating process in which film thickness and consistency is controlled by chuck spin speed and the vapor evacuation rate of the chamber. A pre-exposure bake cycle sets or stabilizes the material. This process has been employed in the manufacture of components in the past decade, notably by *Lumenon Innovative Lightwave Technology, Inc* in the fabrication of integrated photonic devices in hybrid glass/polymer circuits on silicon chips, and gracefully extends to devices on the THz scale. Figure 6 illustrates the sequence of processes in fabricating two turns of helical geometry.

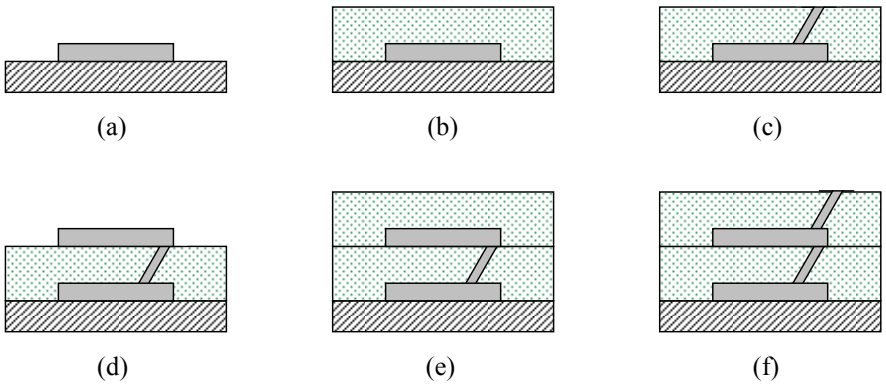


**Figure 6**. Fabrication of helical antenna elements (*a*) first wind is metal on transparent substrate (*b*) transparent layer on first wind (*c*) contact metal through substrate to first wind (*d*) second wind (*e*) transparent layer on second wind (*f*) contact metal through substrate to second wind.

## 3. ANTENNA SIMULATION

Simulation results for the 1 THz helical antenna are now presented to demonstrate electrical properties of the antenna array, radiation pattern, and interference between array elements. Although the planar winding and contact construction appear to be different from a circular helix, electrically it exhibits no difference. Simulation results verify electrical equivalence. Additional windings to the helix enhance the gain, or equivalently, focus the radiation into a smaller angular spread. The array of the helical elements is thus a THz lens or focusing element. With fabrication process of the lens array in place, we demonstrate a layout of the antennas to obtain optimal constructive interference between radiative elements.

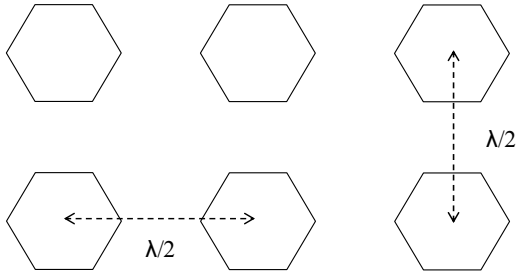


**Figure 7**. Partial helical array shown in XY planar cross-section. Spacing between helix center points is λ/2, 150 μm for the 1 THz model.

Constructive interference may be obtained by spacing elements at multiples of λ/4. Placement on a λ/2 square grid is shown in figure 7. The resulting enhanced gain is shown in the lower part of figure 8.

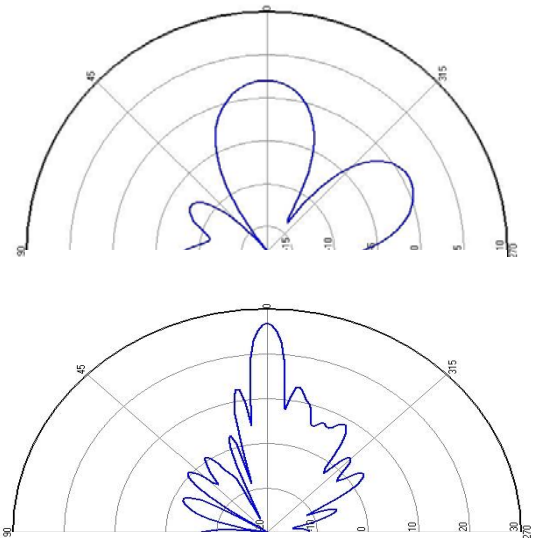

**Figure 8**. Antenna gain for single helix in upper figure (2 dBi maximum). Gain for 16x16 helix array in lower figure with (26 dBi maximum).

The 2 dBi gain for the single helix may be improved with additional windings. The 26 dBi gain achieved by the 16x16 array demonstrates the additive effect produced by the array layout. Both the single helix and 16x16 array were simulated with a flat ground plane; the side lobes seen in the patterns may be reduced through modifications to the ground plane.

The effects of constructive interference on the magnitude of the electric field for an 8x8 helical array are pictured in figure 9. In 9(a) the field surrounding the antenna is guided from a diverging wavefront to a near-planar wavefront. In figure 9(b) it is apparent that the individual fields add in a constructive manner to yield a field strength approaching 0 dB. Field addition is optimized by the unison phasing of the individual sources and the $\lambda/2$ grid spacing.

To obtain a scaling rule for the performance as a function of antenna elements, simulations were run for various array configurations as given in table 3. The figures of merit in the table are the gain and the half-power beam width. The HPBW measures the angular spread between -3 dB points in the antenna gain pattern. As the HPBW decreases with the addition of more antenna elements, the beam is more directive and the gain is increased. The HPBW performance is plotted in figure 10 and antenna array gain in figure 11.

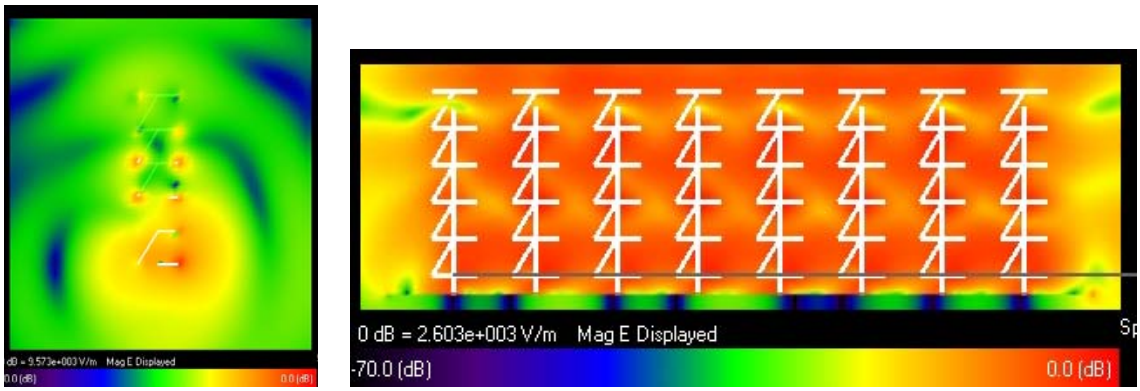


(a) single helical antenna (b) eight by eight helical antenna array

**Figure 9**. Field plots for magnitude of the electric field in YZ planar cross section. Comparison of field strength of helix array to single helix demonstrates constructive interference between array elements. Calibrated color bar at bottom gives the magnitude of the electric field from 0.0 dB (red), -35 dB (green) to -70 dB (black).

**Table 3**. Performance metrics, number of elements, and array configuration.

| **# elements** | **array configuration** | **Gain** dBi | **HPBW** deg |
|---|---|---|---|
| 1 | 1 | 2 | 40 |
| 2 | 1 x 2 | 9 | 30 |
| 4 | 2 x 2 | 12 | 20 |
| 64 | 8 x 8 | 21 | 10 |
| 256 | 16 x 16 | 26 | 2.5 |

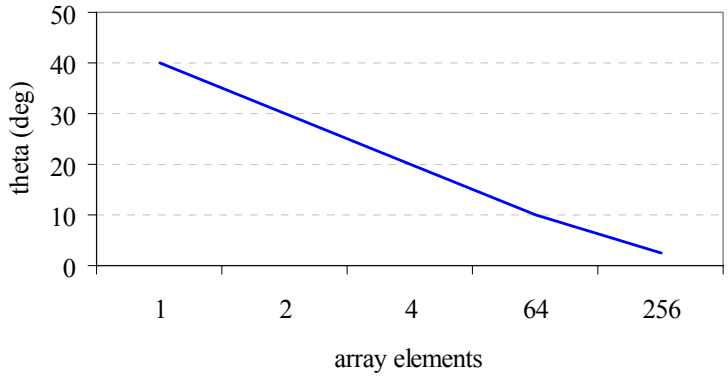


**Figure 10**. HPBW width vs. number of array elements.

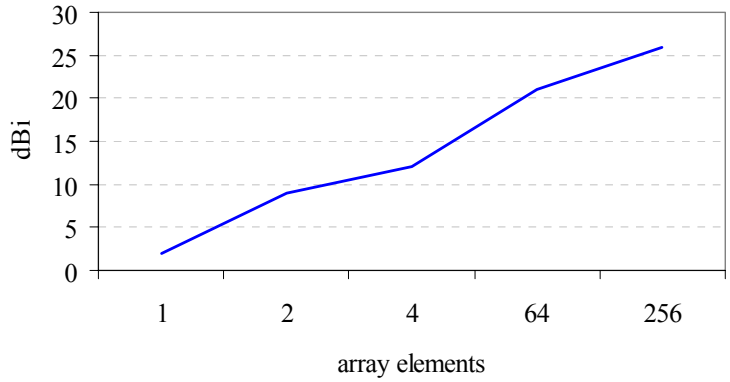


**Figure 11**. Antenna gain (dBi) vs. number of array elements.

## 4. CONCLUSION

Given the favorable simulation results, the APELC SRR and antenna design presents a viable solution for the active element of a compact field-deployable THz source. The Manley-Rowe cascade provides an efficient means of frequency up-conversion to enable wall-plug powering of the device. Improvements to the driver circuitry and conversion process in prototype cycles are expected to allow battery operation for both source and detector modes of operation.

The SRR array provides quasi-monochromatic radiation, with bandwidth determined by the precision of the pattern and etch processes. Detuning of geometry dimensions may be used to obtain a wider spectrum. Driving the SRR array in-phase allows a high degree of partial coherence, thus enabling coherent detection methods for signal extraction from background noise. The helical antenna elements emit and detect circularly polarized light to enable polarized light imaging for enhanced contrast.

Fabrication of THz active element in a monolithic unit greatly simplifies the package. The element may be installed in a modular manner with the driver, power supply and housing to simplify device use and maintenance. The modularity of the active element also enables interchange of elements to obtain different spectra.

As demonstrated, the gain scales exponentially with number of antenna elements. The HPBW or angular spread of the radiation places more energy on target and narrows detection sector in receiver mode. Power per unit area, or intensity, increases exponentially with the number of array components as seen in figure 11. Thus a customer-specified average power may be obtained through increasing component count. The relatively compact footprint of the active element allows growth to significant density on a single substrate as compared to discrete emitters and linear antennas.

## ACKNOWLEDGMENTS

We extend thanks and gratitude to Raymond Luebbers and Ronn Brourman of Remcom for use of the XFDTD software used to develop and corroborate geometries in this paper.

## REFERENCES

[1] *Terahertz for Military and Security Applications III*, edited by R. Jennifer Hwu, Dwight L. Woolard, Mark J. Rosker, **Proceedings of SPIE Vol. 5790**. SPIE Press, Bellingham, WA, 2005, pp 167-179.
[2] *Terahertz and Gigahertz Electronics and Photonics IV***,** edited by R. Jennifer Hwu, Kurt J. Linden. **Proceedings of SPIE Vol. 5727**, SPIE Press, Bellingham, WA, 2005.
[3] Vermont Photonics. *Terahertz Laser Technology*. 05 Jan 2006.<http://www.vermontphotonics.net/index2.html>.
[4] V.G. Veselago. *The Electrodynamics of substances with simultaneously negative values of ε and μ.* Soviet Physics, Volume 10, No. 4. January-February 1968.

[5] David R. Smith and Norman Kroll. *Negative Refractive Index in Left-handed materials*. Physical Review Letters, Volume 85, No. 14. October 2000.
[6] John Pendry. *Manipulating the Near Field with Metamaterials*. Optics & Photonics News, Optical Society of America, September 2004.
[7] Yen et al. *Terahertz Magnetic Response from Artificial Materials*. Science, pp.1494-1496. 5 March 2004.
[8] James T. Coleman. **Microwave devices**. Reston Publishing (Prentice-Hall), 1981.
[9] Joseph F. White. **High Frequency Techniques**. Wiley Interscience, 2004.
[10] S.C. Hagness et al. *FDTD Microcavity Simulations: Design and Experimental Realization of Waveguide-coupled single-mode ring and Whispering-Gallery-Mode Disk Resonators*. IEEE Journal of Lightwave Technology, Vol. 15 No. 11, November 1997.
[11] J.B Pendry et al. *Magnetism from Conductors and Enhanced nonlinear Phenomena*. IEEE Transactions on Microwave Theory and Techniques, Vol. 47, No. 11, November 1999.
[12] Ekmel Ozbay et al. *Transmission and Reflection Properties of Composite Double Negative Metamaterials in Free Space.* IEEE Transactions on Antennas and Propagation, Vol. 51, No. 10, October 2003.
[13] Stefan linden et al. *Magnetic Response of Metamaterials at 100 Terahertz*. ***Science*** 19 November 2004: Vol. 306. no. 5700, pp. 1351 – 1353.
[14] Ricardo Marqués et al. *Comparative Analysis of Edge- and Broadside-coupled Split Ring Resonators for Metamaterial Design-Theory and Experiments*. IEEE Transactions on Antennas and Propagation, Vol. 51, No. 10, October 2003.
[15] John D. Kraus. **Antennas**, 2nd edition. McGraw-Hill, 1988.
[16] *3-D Helical THz Antennas Directly on Semiconductor Substrates*. Electrical and Computer Engineering Department, The University of New Mexico. 06 January 2006. <www.eece.unm.edu>.
[17] S. I. Najafi et al. *Sol-gel glass waveguide and grating on silicon*. IEEE Journal of Lightwave Technology, Volume: 16 , Issue: 9, pp: 1640 – 1646. September 1998.